PHYSICAL SCIENCE

10.1126/sciadv.1601072

Direct carbon-carbon coupling of furanics with acetic acid over Brønsted zeolites

Abhishek Gumidyala, Bin Wang, Steven Crossley*

Effective carbon-carbon coupling of acetic acid to form larger products while minimizing CO_2 emissions is critical to achieving a step change in efficiency for the production of transportation fuels from sustainable biomass. We report the direct acylation of methylfuran with acetic acid in the presence of water, all of which can be readily produced from biomass. This direct coupling limits unwanted polymerization of furanics while producing acetyl methylfuran. Reaction kinetics and density functional theory calculations illustrate that the calculated apparent barrier for the dehydration of the acid to form surface acyl species is similar to the experimentally measured barrier, implying that this step plays a significant role in determining the net reaction rate. Water inhibits the overall rate, but selectivity to acylated products is not affected. We show that furanic species effectively stabilize the charge of the transition state, therefore lowering the overall activation barrier. These results demonstrate a promising new route to C–C bond–forming reactions for the production of higher-value products from biomass.

INTRODUCTION

Heteroaromatic functionalization via Friedel-Crafts acylation to attach a carbonyl group to the aromatic rings is important for the production of several specialty chemicals and drugs (*1*). Acylation is commonly carried out with acyl chlorides or anhydrides as acylating agents because of their ease of activation. Although efforts have been made to use carboxylic acids directly to minimize waste and improve efficiency, the more severe conditions that are required often lead to undesired side reactions with negative consequences for specialty chemical synthesis. Studies carried out with the direct use of carboxylic acids as acylating agents are therefore the vast minority, with a nearly nonexistent understanding of the consequential influence of water on the said reaction rates.

However, to upgrade biomass streams, the direct activation of acetic acid, which is the most abundant compound present in many biomass-derived streams (*2*, *3*), may be a prerequisite to obtain adequate yields of high-value products. The efficient conversion of molecules present in streams derived from biomass to useful fuel and chemical precursors is a daunting task. Thermochemical routes, such as pyrolysis, torrefaction, and solvolysis that transform the polymers in lignocellulosic biomass to monomeric species yield a complex mixture of chemically incompatible compounds (*4*–*9*). Although mild thermal approaches, such as torrefaction, can selectively decompose hemicellulose and cellulose, this still yields a blend of furanic and carboxylic acid species that are difficult to separate (*8*, *9*). The acidity introduced by acetic acid facilitates the polymerization of furanic species at room temperature, creating obvious storage and transportation challenges (*2*, *3*, *8*, *10*–*12*).

Stabilization through severe hydrodeoxygenation decomposes these acids, which consist predominantly of acetic acid, to low-value C_1- and C_2-containing species. Although this approach yields a stable product, the excessive requirement of hydrogen and the low yield of products that are liquid at room temperature hinder the economics of the overall process (*13*–*15*). Excessively high temperatures with acid catalysts, with the aim of producing deoxygenated products, suffer from similar consequences of excessive amounts of carbon wasted as coke and light compounds.

One promising route to improve yields is to couple carboxylic acids, predominantly acetic acid, in the vapor phase to produce larger products. Decarboxylative ketonization is one route that has received a great deal of attention to stabilize these acids to form ketones that can undergo sequential coupling, such as aldol condensation, to generate useful compounds (*16*–*20*). Perhaps the most significant drawback of this reaction is the stoichiometric formation of carbon dioxide as a by-product, corresponding to 25% of the carbon in the acetic acid. An alternative approach to prestabilizing the blend of oxygenates via selective C–C coupling of acids and furanic compounds while yielding thermally stable intermediates would lead to a step change in the field.

Direct dehydration of acetic acid to form acyl intermediates followed by coupling to a furanic substrate would be very appealing. Friedel-Crafts acylation has been the subject of several reviews, with the vast majority of studies concerning carboxylic acids focused on coupling with aromatic or phenolic compounds in the absence of cofed water for specialty chemical synthesis (*1*, *21*, *22*). Furanic species have been shown to couple with acetic anhydride under very mild anhydrous conditions (*23*), but direct coupling of furanic species, such as furan or 2-methylfuran (2-MF) with acetic acid has not been reported. Furanic species are known to undergo a wide range of side reactions over Brønsted acid sites, many of which can lead to uncontrolled polymerization and coke formation (*24*).

Here, we report the direct vapor-phase coupling of acetic acid with furanic species over HZSM-5 zeolites, resulting in fuel range products without losing CO_2 in the process and increasing the overall amount of carbon in the biomass retained in transportation fuel precursors in the form of C–C bonds (*25*, *26*). 2-MF is chosen as a probe molecule because it can be generated from the selective C–O cleavage of furfural (*27*), which is abundant in biomass degradation streams. Under milder conditions than necessary for ketonization, acylation of 2-MF occurs with high selectivity under a wide range of concentrations. The kinetics of this reaction and the influence of water on the reaction rate are discussed. Temperature-programmed desorption (TPD)

School of Chemical, Biological and Materials Engineering, The University of Oklahoma, Norman, OK 73019, USA.
*Corresponding author. Email: stevencrossley@ou.edu

experiments and density functional theory (DFT) calculations are used to explain the mechanism of this promising reaction, highlighting the important role of confinement on the overall reaction and the acyl formation step. Finally, we demonstrate the important influence of MF on the stabilization of the charge of the acylium ion at the transition state, which facilitates C–C bond formation. These results have a broader influence on C–C coupling through Friedel-Crafts reactions over zeolites.

RESULTS

Evidence for direct acylation of furanics and reaction kinetics

A schematic of the direct acylation of 2-MF with acetic acid over HZSM-5 is shown in Fig. 1A. The resulting product—acetyl MF—contains significance both as a specialty chemical and as a fuel precursor. By saturating the surface of HZSM-5 (SiO_2/Al_2O_3 = 80; CBV8014, Zeolyst International) with acetic acid followed by ramping up the temperature, two distinct regimes have been reported (*28*). The first step involves the dehydration of the acid to form acyl species. Upon subsequent heating of the sample, these acyl species interact further with activated carboxylic acids to form ketone products. The latter step has a greater activation energy and can be avoided by operating at lower temperatures.

Evidence for direct acylation with furanic species via acetic acid can be obtained by conducting a similar experiment while pulsing MF across a surface populated with acyl groups. Saturating an HZSM-5 catalyst surface with acetic acid at 100°C in a TPD system (see section S1.2 for the experimental setup) followed by ramping up the temperature to 220°C results in dehydration of acids to produce surface acyl species. Observation of self-coupling of acetic acid does not begin to occur until 250°C (*28*). Results of product evolution following MF pulses across the acyl-saturated catalyst at 220°C are shown in Fig. 1B. With each pulse of 2-MF, acetyl MF is observed desorbing from the catalyst surface. The peak intensity decays with increasing pulse number, indicating a drop in the amount of acylation products formed, likely due to an extinction of surface acyl species. This experiment suggests that acetic acid dehydrates on a Brønsted acid site to form surface acyl species that attack the ring of 2-MF.

The acylation of 2-MF with acetic acid occurs over the same HZSM-5 catalyst at temperatures ranging from 220° to 300°C in an atmospheric pressure fixed-bed flow reactor. This reaction is exclusively selective to acetyl MF isomers over a broad range of temperatures. Conversions, selectivity, and yields for all the reactions are given in Fig. 2D. Product yield is dominated by acetyl MF isomers, with detectable concentrations of acetone observed at a reaction temperature of 300°C. The carbon balance for each of the reactions tabulated in Fig. 2D is more than 95% (detailed calculations for all the reactions are tabulated in the Supplementary Materials). The furan ring is predominantly acylated at the ortho position, forming 2-acetyl-5-MF, although traces of 3-acetyl-5-MF are produced, with selectivity to the latter increasing at elevated temperatures. A minor increase in the selectivity to 3-acetyl-5-MF, from ~4 to 12% of the acylated products, is observed with an increase in temperature, suggesting a higher barrier to acylate in this position.

The acylation reaction order was estimated at a reaction temperature of 250°C by independently varying the concentration of acetic acid and 2-MF. As shown in Fig. 2 (A and B), the reaction is first order with respect to both reactants. Furthermore, the effect of water was studied by cofeeding water with 2-MF and acetic acid. As seen in Fig. 2C, water inhibits acylation with an order of −0.7. This does not preclude biomass-derived streams that include water in the vapor phase, because increasing concentrations of water, even if they exceed 2-MF concentrations in the feed, appear to have no detrimental influence on the catalyst's selectivity or stability (fig. S4). Under more severe temperatures where an abundance of ketenes may be present, water has been shown to inhibit catalyst deactivation for acid coupling

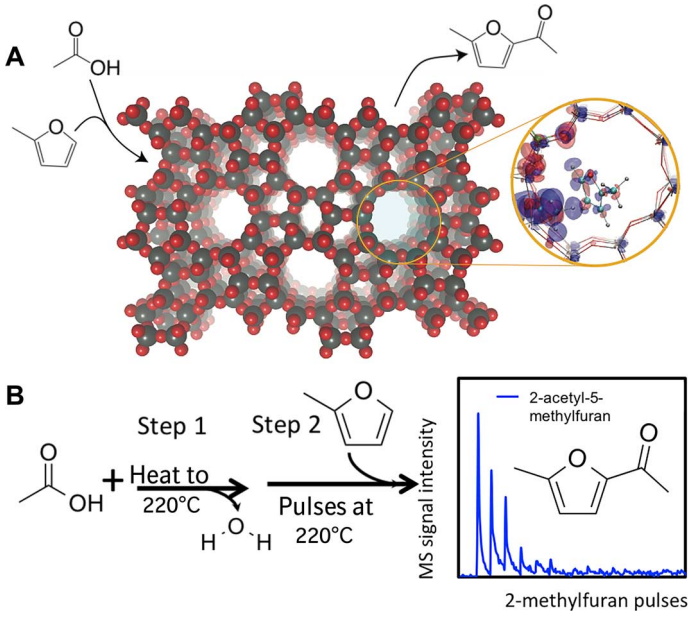

Fig. 1. Direct acylation of MF with acetic acid over HZSM-5. (**A**) Schematic of 2-MF acylation with acetic acid over HZSM-5. (**B**) TPD experiment over HZSM-5 showing 2-acetyl-5-MF desorbing with 2-MF pulses from catalyst bed saturated with surface acyl species at 220°C.

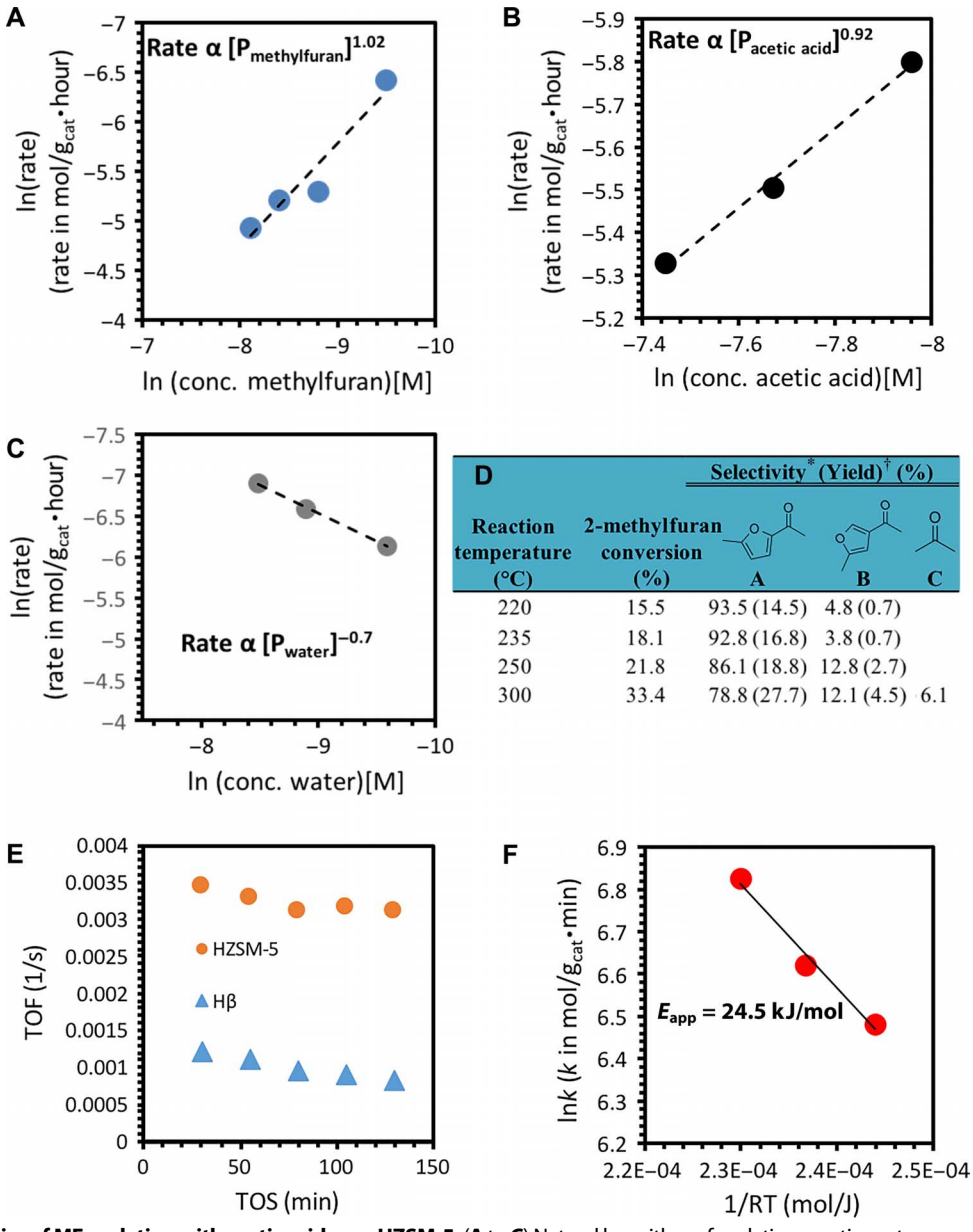

Fig. 2. Reaction kinetics of MF acylation with acetic acid over HZSM-5. (**A** to **C**) Natural logarithm of acylation reaction rate versus concentration of acetic acid (A), concentration of 2-MF (B), and concentration of water (C) over CBV8014 with 0.0198 mmol of catalyst at a reaction temperature of 250°C and 30-min time on stream. The included table (**D**) shows conversion, product yields, and product selectivities observed upon passing 2-MF and acetic acid over HZSM-5 after 30-min time on stream with a constant 0.0198 mmol of Brønsted site catalysts. An acetic acid–to–2-MF mole ratio of 1:0.258 was used in this study, with a catalyst mass of 0.05 mg. *Selectivity$(\%) = \frac{\text{moles of the product produced}}{\text{moles of 2-MF consumed}} \times 100$; †Yield$(\%) = \frac{\text{moles of product produced}}{\text{moles of 2-MF fed}} \times 100$. (**E**) TOF of 2-MF acylation with acetic acid over HZSM-5 and Hβ as a function of time at 250°C and 0.05 mg of catalyst. (**F**) Apparent activation energy of acetic acid acylation over HZSM-5 estimated for a temperature range of 220° to 250°C. The molar feed rate of acetic acid (0.00437 mol/hour) and 2-MF (0.00113 mol/hour) with 0.0198 mmol of catalyst was used to obtain apparent activation energies.

reactions (*28*). The enhancement in stability was explained by the potential reaction of water with trace ketene species in the gas phase that can lead to rapid catalyst deactivation.

The role of zeolite topology was investigated by comparing the catalytic activity over HZSM-5 to that over Hβ zeolite (SiO_2/Al_2O_3 = 38; CP814C, Zeolyst International). Figure 2E shows the turnover frequency (TOF) for 2-MF acylation with acetic acid over these two zeolites. HZSM-5 has far better activity in comparison with the larger-pored Hβ.

The apparent activation energy for acylation was estimated using an Arrhenius plot over the temperature range of 220° to 250°C. The obtained apparent activation energy corresponds only to acylation reaction, because no side reactions were observed under these conditions. As shown in Fig. 2F, the estimated apparent barrier is 24.5 kJ/mol. By contrast, the apparent energy for the ketonization of acetic acid over HZSM-5 was 67 kJ/mol (fig. S9). We have previously shown that acetic acid selectively undergoes decarboxylative ketonization at temperatures

above 250°C in the absence of a coreactant that may react with surface acyl species. TPD experiments and infrared spectroscopy reveal an initial dehydration step that produces surface-bound acyl species on Brønsted acid sites of HZSM-5. The acetone reported in this study at 300°C is due to this ketonization reaction. The apparent barrier for acylation is significantly lower than that of ketonization, which could suggest that the energy required to couple an acyl with 2-MF is significantly lower than that required to couple an acyl with a carboxylic acid to yield a β-keto acid once adsorption energies are considered.

Evaluating reaction energies from DFT

Further information regarding the coupling pathway and resulting energetics is gained through dispersion-corrected DFT calculations (see detailed methods in the Supplementary Materials). Hybrid functional calculations have also been performed because DFT calculations may underestimate the reaction barriers caused by the charge delocalization error of the approximate exchange-correlation functionals (*29*). The whole acylation reaction occurs on two oxygen atoms bound to the same Al atom (Fig. 3). First, acetic acid adsorbs on HZSM-5 by forming hydrogen bonds with Brønsted acid sites, and subsequently, acyl species and water form, with a true energy barrier of 104 kJ/mol or an apparent barrier of 16 kJ/mol due to the very exothermic adsorption of acetic acid resulting from both the H-bond and the structural confinement. We obtain an enhanced apparent barrier of 40 kJ/mol using the hybrid functional (*30*, *31*). Notably, all of the calculated adsorption enthalpy values are very similar between DFT and hybrid calculations, whereas the transition states are more stabilized by the semilocal Perdew-Burke-Ernzerhof (PBE) functional (*32*) because of the charge delocalization. The experimentally obtained apparent activation energy of 24.5 kJ/mol, while first order with respect to the reactants (Fig. 2), agrees well with the apparent barrier from DFT and hybrid functional calculations, suggesting that the acyl formation step plays an important role in the overall reaction rate. The rapid evolution of acetyl MF upon pulsing 2-MF over an isothermal acyl-covered surface (Fig. 1B) also indicates that C–C coupling between MF and a surface acyl exhibits a lower barrier than acetic acid self-coupling. However, it is important to note that the reaction behaves as first order with respect to 2-MF. It is possible that both the reversible acyl formation and subsequent C–C coupling steps significantly contribute to controlling the net rate, the exact degree of which should be the focus of future studies (*33*). Contrasting these results with those observed over Hβ zeolite (fig. S8), the adsorption of acetic acid is more strongly stabilized in HZSM-5. This subsequently leads to a higher activation energy barrier for Hβ when referencing the gas-phase acid and the transition state for acyl formation. Because this step appears to play an important role in the overall rate of reaction, all subsequent discussion will focus on HZSM-5.

When 2-MF is introduced, it reacts with the surface acyl group to form an intermediate species, which is deprotonated subsequently to recover both the molecular aromaticity and the Brønsted acid site, leading to a large energy gain. The barrier of formation of 2-acetyl-5-MF from 2-MF and acyl is less than that of acyl formation. This is in contrast to the ketonization reaction, where the C–C coupling step exhibits the highest barrier.

The direct desorption of the acyl species in the absence of 2-MF is very endothermic, with an energy cost of 116 kJ/mol, which is much larger than the true activation barrier of 76 kJ/mol for the C–C coupling step. Figure 4A shows the charge transfer between the complex (the desorbed acyl and 2-MF) and the zeolite framework in the transition state of the C–C coupling step. To compensate for the charge in the zeolite framework, a certain number of electrons flow from the complex to zeolite, evidenced by the charge depletion in the desorbed acyl and the 2-MF molecule and by the charge accumulation at the

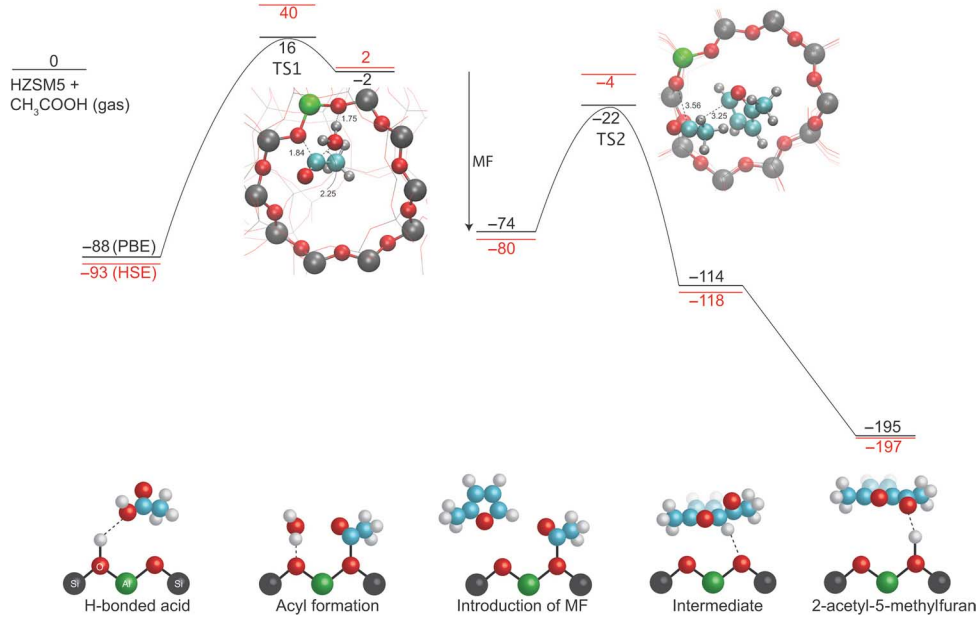

Fig. 3. DFT calculations of acylation of 2-MF with acetic acid. All the values are reported in kilojoules per mole. The transition states are shown as the insets with C, O, H, Si, and Al atoms colored cyan, red, gray, black, and green, respectively. The results calculated using the Heyd-Scuseria-Ernzerhof (HSE) hybrid functional (red) are also shown, for comparison with the PBE results (black). The reaction path is schematically shown at the bottom.

oxygen atoms bonded to the Al. Integration of the charges via Bader analysis yields a total number of electron transfer of 1.2 electrons to the zeolite framework, including 0.6 electrons from the desorbed acyl (acylium ion) (Fig. 4C) and 0.6 electrons from 2-MF. In the absence of MF, the integrated charge of 1.2 electrons is located at the acylium ion (Fig. 4D). In addition, the interaction between the acylium ion and the 2-MF molecule broadens the occupied states (close to the Fermi level) of the acylium ion, as shown in the Projected Density of States in Fig. 4E. This charge delocalization and electronic hybridization caused by 2-MF in the proximity stabilizes the acylium ion and lowers the activation barrier in the C–C coupling step.

DISCUSSION

The results presented here illustrate the stable and selective C–C coupling of two biomass-derived species (acetic acid and 2-MF) that lead to polymerization and coke formation when introduced alone to

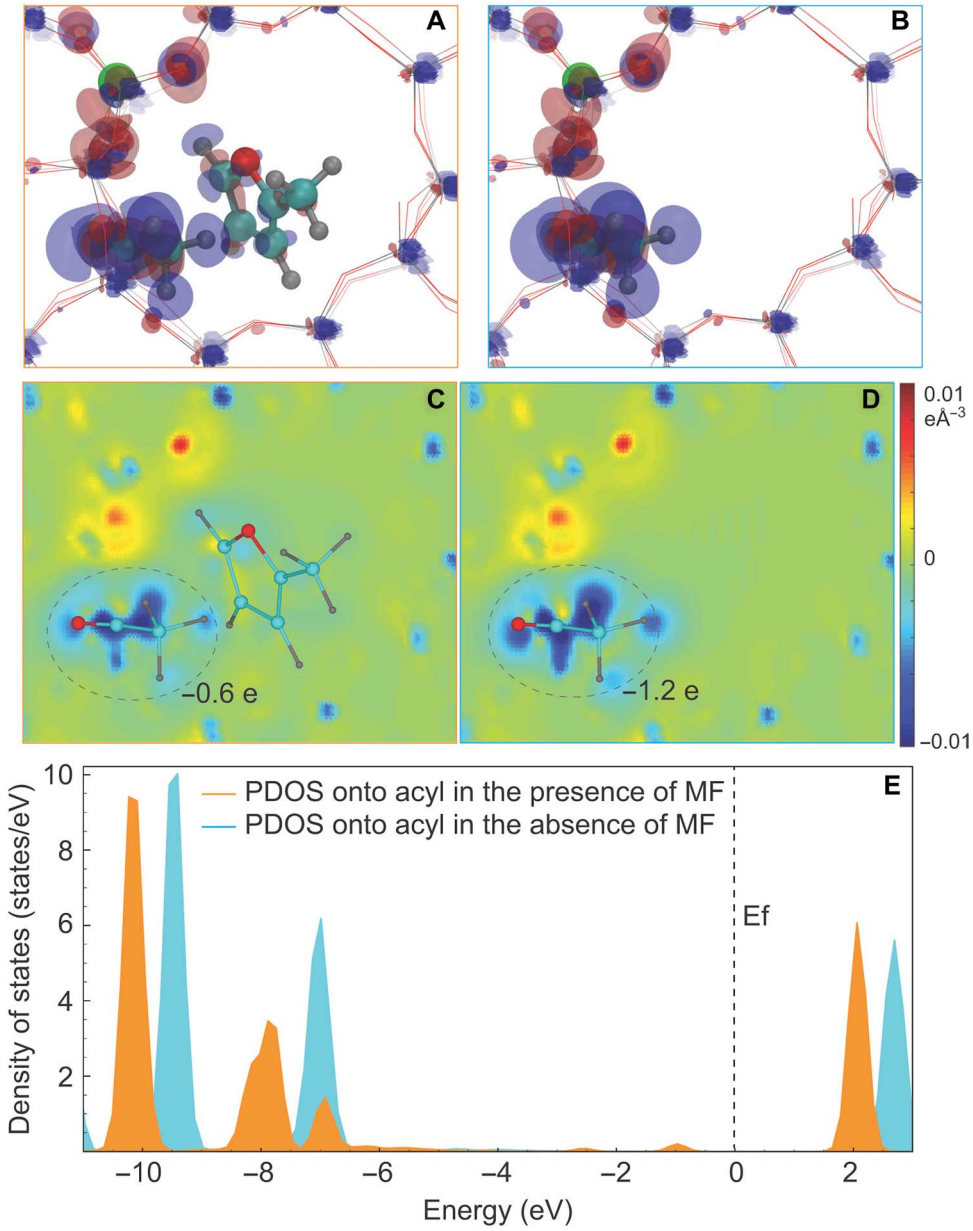

Fig. 4. Charge transfer and density of states calculated using the hybrid functional. (**A**) Charge transfer between the molecules (the desorbed acyl and 2-MF) and the zeolite framework in the transition state of the C–C coupling step. (**B**) The same charge transfer in the absence of the 2-MF molecule. Red and blue indicate charge accumulation (negative charge) and charge depletion (positive charge), respectively. The isosurface corresponds to a charge density of ±0.015 e Å^{-3}. (**C** and **D**) Plane-averaged charge transfer (see the methods in the Supplementary Materials) of the same area as in (A) and (B). Electron depletion at the desorbed acyl (indicated by dashed circles) via the Bader charge analysis. (**E**) Projected density of states (PDOS) onto the desorbed acyl species (acylium ion) in (A) and (B).

Brønsted zeolite catalysts (*28*, *34*). This is a promising new route for the conversion of biomass-derived streams to higher-value fuels and chemicals without sacrificing carbon as CO_2 in the process. Alternative approaches to upgrading acetic acid, such as ketonization, exhibit a larger apparent barrier for C–C coupling. The high abundance of surface acyl groups present when acetic acid is introduced alone to a zeolite is in equilibrium with ketene species, leading to uncontrollable coke formation and catalyst deactivation (*28*). Furanic species are known to polymerize over Brønsted acid sites even under ambient conditions (*34*). In the scenario presented here, the low activation barrier for 2-MF coupling to acyl species allows for the stable production of C–C bonds while avoiding these undesired side reactions.

Flow reaction studies show that the direct acylation of 2-MF with acetic acid over HZSM-5 is a relatively stable reaction, to produce predominantly 2-acetyl-5-MF. Acetone is observed as a side product with insignificant concentrations at temperatures below 300°C, under the reactant concentrations used here. Water inhibits the rate but does not detrimentally influence selectivity. Furthermore, as shown with high partial pressures of acetic acid, water may improve catalyst stability at higher temperatures (*28*). Streams consisting primarily of acetic acid, furfural, and water can be produced from the torrefaction of lignocellulosic biomass (*25*), and the conversion of furfural has been shown to selectively produce furan or 2-MF over a variety of catalysts (*27*, *35*). It should be noted that furfural conversion has been shown to not be inhibited by the presence of acetic acid (*36*). This implies that this selective acylation reaction could be applied to upgrade biomass-derived streams containing water.

Results in Fig. 2E emphasize the importance of topology for this reaction. HZSM-5, with a smaller pore size than Hβ zeolites, exhibits a higher TOF and improved catalyst stability for this reaction. Upon studying the acylation of phenol with zeolites, Padró and Apesteguía (*37*) also reported the superior performance of HZSM-5 compared to larger-pored HY zeolites. This suggests that confinement plays an important role in this reaction.

Charge analysis from DFT (Fig. 4) implies that the ability of the MF molecule to compensate for the charge of the acylium ion in the transition state may significantly reduce the barrier for C–C coupling. In the case of 2-MF, the reduction in the barrier is significant enough to make the rate of acid dehydration a kinetically relevant step. This could explain the stability of the catalyst under these conditions, because the rapid coupling of 2-MF with surface acyl groups will decrease the population of surface acyl species that could otherwise convert to ketenes and, subsequently, carbonaceous deposits. In addition, low partial pressures of 2-MF and a high coverage of acetic acid will likely prevent the excessive furan polymerization over Brønsted zeolites. These calculations demonstrate the importance of the ability of 2-MF to stabilize the charge of the acylium ion at the transition state, which may be generally true for other C–C coupling reactions involving a charged species.

MATERIALS AND METHODS

A typical procedure for gas acylation flow reactions of 2-MF with acetic acid over HZSM-5 is as follows. A catalyst was packed between quartz wool in a $^1/_4$-inch quartz reactor and pretreated at 300°C for 1 hour under a helium flow of 125 ml/min to remove physisorbed water. A thermocouple was attached to the outside wall of the reactor near the catalyst bed to maintain the reactor temperature. After pretreatment, the temperature was adjusted to the required reaction temperature, and reactants were fed through a syringe pump. The inlet of the reactor was heated to create a vaporization zone for the reactants, and the outlet of the reactor and downstream lines were heated to 250°C to prevent condensation of products. Samples were taken via a six-port valve connected to an HP 6890GC instrument equipped with a flame ionization detector and an INNOWax column for analysis.

TPD studies of reactants are performed in the same system used for isopropylamine (IPA) TPD (see section S1.2 for details). The catalyst bed was pretreated under a helium flow of 20 ml/min at 300°C for 1 hour, and then the temperature was lowered to 100°C. Several 2-μl pulses of acetic acid was injected into the reactor using a syringe, and saturation of the catalyst bed was ensured by following $m/e = 60$ in mass spectrometry (MS). This was followed by flushing for 2 hours in helium to remove physisorbed acetic acid, after which temperature was ramped up to 220°C using a steady ramp rate of 10°C/min. Then, MF was pulsed, and the products were tracked using MS.

DFT calculations were carried out using the VASP (Vienna ab initio simulation) package (*38*). The PBE generalized gradient approximation exchange-correlation potential (*32*) was used, and the electron-core interactions were treated in the projector augmented wave method (*39*, *40*). The van der Waals interaction was taken into account through the so-called DFT-D3 semiempirical methods via a pairwise force field (*41*, *42*). An HSE hybrid functional (*30*, *31*) was also used to calculate the total energy of the initial, transition, and final states that were already optimized by DFT-D3 calculations to reduce underestimation of the reaction barriers caused by the charge delocalization error of the local and semilocal exchange-correlation functionals (*29*). The nudged elastic band (*43*) method was used to find the transition state and calculate the reaction barriers. The transition states were further verified by vibrational calculations.

All the calculations were performed using a ZSM-5 unit cell including ^{96}Si and ^{192}O atoms. One Si atom at the T12 site, which was located at the intersection and more accessible to reactions (*44*), was replaced by one Al atom; thus, the Si/Al ratio is 95:1. The proton was initially attached to the O atom that was between the Al atom and the nearest T12 Si atom. The structure of the unit cell was taken from an experimental work ($a = 20.078$ Å; $b = 19.894$ Å; $c = 13.372$ Å) (*45*) and fixed during the calculation. Atomic relaxation was performed using a single Γ point of the Brillouin zone with a kinetic cutoff energy of 400 eV. A further increase of k-point sampling to ($1 \times 1 \times 2$) does not change the reaction energetics. All the atoms (zeolite and the molecules) were fully relaxed until the atomic forces were smaller than 0.02 eV Å^{-1}.

SUPPLEMENTARY MATERIALS

Supplementary material for this article is available at http://advances.sciencemag.org/cgi/content/full/2/9/e1601072/DC1

Supplementary Information

fig. S1. IPA TPD profile of CBV8014 and CPC814C, showing the evolution of IPA, propylene, and ammonia as a function of temperature.

fig. S2. Scanning electron microscopy image of CBV8014 to estimate the crystal size of the catalyst.

fig. S3. X-ray diffraction data for CBV8014, showing that the sample is a crystalline zeolite with MFI framework type.

fig. S4. Comparing TOF with increasing water cofeeding at a reaction temperature of 250°C.

fig. S5. Comparing TOF with increasing partial pressure of 2-MF at a reaction temperature of 250°C.
fig. S6. Comparing rate of acylation between CBV80114 and Na-exchanged CBV8014 to test internal diffusion limitations.
fig. S7. Optimized structures from DFT calculations.
fig. S8. DFT calculations of acyl formation from acetic acid in Hβ.
fig. S9. Apparent activation energy of acetic acid ketonization over CBV8014 estimated for a temperature range of 270° to 310°C.
fig. S10. Comparing the conversion of MF by using different catalyst amounts.
fig. S11. Online gas chromatography–flame ionization detector spectrum for MF acylation with acetic acid at a conversion level of 15%.
fig. S12. Gas chromatography–MS spectrum to identify compounds of MF acylation reaction with acetic acid.
References (*46*, *47*)

REFERENCES AND NOTES

1. G. Sartori, R. Maggi, Use of solid catalysts in Friedel–Crafts acylation reactions. *Chem. Rev.* **111**, PR181–PR214 (2011).
2. S. Czernik, A. V. Bridgwater, Overview of applications of biomass fast pyrolysis oil. *Energy Fuels* **18**, 590–598 (2004).
3. A. Oasmaa, D. C. Elliott, J. Korhonen, Acidity of biomass fast pyrolysis bio-oils. *Energy Fuels* **24**, 6548–6554 (2010).
4. M. Stöcker, Biofuels and biomass-to-liquid fuels in the biorefinery: Catalytic conversion of lignocellulosic biomass using porous materials. *Angew. Chem. Int. Ed. Engl.* **47**, 9200–9211 (2008).
5. Q. Zhang, J. Chang, T. Wang, Y. Xu, Review of biomass pyrolysis oil properties and upgrading research. *Energy Convers. Manage* **48**, 87–92 (2007).
6. A. V. Bridgwater, G. V. C. Peacocke, Fast pyrolysis processes for biomass. *Renewable Sustainable Energy Rev.* **4**, 1–73 (2000).
7. S. Wan, C. Waters, A. Stevens, A. Gumidyala, R. Jentoft, L. Lobban, D. Resasco, R. Mallinson, S. Crossley, Decoupling HZSM-5 catalyst activity from deactivation during upgrading of pyrolysis oil vapors. *ChemSusChem* **8**, 552–559 (2015).
8. J. Meng, J. Park, D. Tilotta, S. Park, The effect of torrefaction on the chemistry of fast-pyrolysis bio-oil. *Bioresour. Technol.* **111**, 439–446 (2012).
9. M. J. Prins, K. J. Ptasinski, F. J. J. G. Janssen, Torrefaction of wood: Part 2. Analysis of products. *J. Anal. Appl. Pyrol.* **77**, 35–40 (2006).
10. T. R. Carlson, T. P. Vispute, G. W. Huber, Green gasoline by catalytic fast pyrolysis of solid biomass derived compounds. *ChemSusChem* **1**, 397–400 (2008).
11. D. M. Alonso, J. Q. Bond, J. A. Dumesic, Catalytic conversion of biomass to biofuels. *Green Chem.* **12**, 1493–1513 (2010).
12. J.-P. Lange, Lignocellulose conversion: An introduction to chemistry, process and economics. *Biofuels, Bioprod. Biorefin.* **1**, 39–48 (2007).
13. C.-H. Zhou, X. Xia, C.-X. Lin, D.-S. Tong, J. Beltramini, Catalytic conversion of lignocellulosic biomass to fine chemicals and fuels. *Chem. Soc. Rev.* **40**, 5588–5617 (2011).
14. D. C. Elliott, T. R. Hart, Catalytic hydroprocessing of chemical models for bio-oil. *Energy Fuels* **23**, 631–637 (2008).
15. R. J. French, J. Hrdlicka, R. Baldwin, Mild hydrotreating of biomass pyrolysis oils to produce a suitable refinery feedstock. *Environ. Prog. Sustainable Energy* **29**, 142–150 (2010).
16. T. N. Pham, T. Sooknoi, S. P. Crossley, D. E. Resasco, Ketonization of carboxylic acids: Mechanisms, catalysts, and implications for biomass conversion. *ACS Catal.* **3**, 2456–2473 (2013).
17. T. N. Pham, D. Shi, T. Sooknoi, D. E. Resasco, Aqueous-phase ketonization of acetic acid over Ru/TiO_2/carbon catalysts. *J. Catal.* **295**, 169–178 (2012).
18. M. Vervecken, Y. Servotte, M. Wydoodt, L. Jacobs, J. A. Martens, P. A. Jacobs, in *Chemical Reactions in Organic and Inorganic Constrained Systems* (Springer Netherlands, 1986), pp. 95–114.
19. R. Pestman, R. M. Koster, A. vanDuijne, J. A. Z. Pieterse, V. Ponec, Reactions of carboxylic acids on oxides: 2. Bimolecular reaction of aliphatic acids to ketones. *J. Catal.* **168**, 265–272 (1997).
20. C. D. Chang, N. Y. Chen, L. R. Koenig, D. E. Walsh, Synergism in acetic acid/methanol reactions over ZSM-5 zeolites. *Prepr. Pap. Am. Chem. Soc. Div. Fuel Chem.* **28**, 146–152 (1983).
21. D. E. Resasco, B. Wang, S. Crossley, Zeolite-catalysed C–C bond forming reactions for biomass conversion to fuels and chemicals. *Catal. Sci. Technol.* **6**, 2543–2559 (2016).
22. G. Sartori, R. Maggi, *Advances in Friedel-Crafts Acylation Reactions: Catalytic and Green Processes* (CRC Press, 2009).
23. P. R. Reddy, M. Subrahmanyam, S. J. Kulkarni, Vapour phase acylation of furan and pyrrole over zeolites. *Catal. Lett.* **54**, 95–100 (1998).
24. T. V. Bui, S. Crossley, D. E. Resasco, C–C coupling for biomass-derived furanics upgrading to chemicals and fuels, in *Chemicals and Fuels from Bio-Based Building Blocks*, F. Cavani, S. Albonetti, F. Basile, A. Gandini, Eds. (Wiley-VCH Verlag and Co. KGaA, 2016), pp. 431–494.
25. D. E. Resasco, S. P. Crossley, Implementation of concepts derived from model compound studies in the separation and conversion of bio-oil to fuel. *Catal. Today* **257**, 185–199 (2015).
26. P. Gallezot, Conversion of biomass to selected chemical products. *Chem. Soc. Rev.* **41**, 1538–1558 (2012).
27. S. Sitthisa, W. An, D. E. Resasco, Selective conversion of furfural to methylfuran over silica-supported Ni–Fe bimetallic catalysts. *J. Catal.* **284**, 90–101 (2011).
28. A. Gumidyala, T. Sooknoi, S. Crossley, Selective ketonization of acetic acid over HZSM-5: The importance of acyl species and the influence of water. *J. Catal.* **340**, 76–84 (2016).
29. A. J. Cohen, P. Mori-Sánchez, W. Yang, Insights into current limitations of density functional theory. *Science* **321**, 792–794 (2008).
30. J. Heyd, G. E. Scuseria, M. Ernzerhof, Erratum: "Hybrid functionals based on a screened Coulomb potential"[J. Chem. Phys. 118, 8207 (2003)]. *J. Chem. Phys.* **124**, 219906 (2006).
31. J. Heyd, G. E. Scuseria, M. Ernzerhof, Hybrid functionals based on a screened Coulomb potential. *J. Chem. Phys.* **118**, 8207–8215 (2003).
32. J. P. Perdew, K. Burke, M. Ernzerhof, Generalized gradient approximation made simple. *Phys. Rev. Lett.* **77**, 3865–3868 (1996).
33. C. Stegelmann, A. Andreasen, C. T. Campbell, Degree of rate control: How much the energies of intermediates and transition states control rates. *J. Am. Chem. Soc.* **131**, 8077–8082 (2009).
34. Y.-T. Cheng, G. W. Huber, Chemistry of furan conversion into aromatics and olefins over HZSM-5: A model biomass conversion reaction. *ACS Catal.* **1**, 611–628 (2011).
35. S. Sitthisa, D. E. Resasco, Hydrodeoxygenation of furfural over supported metal catalysts: A comparative study of Cu, Pd and Ni. *Catal. Lett.* **141**, 784–791 (2011).
36. W. Yu, Y. Tang, L. Mo, P. Chen, H. Lou, X. Zheng, One-step hydrogenation–esterification of furfural and acetic acid over bifunctional Pd catalysts for bio-oil upgrading. *Bioresour. Technol.* **102**, 8241–8246 (2011).
37. C. L. Padró, C. R. Apesteguía, Gas-phase synthesis of hydroxyacetophenones by acylation of phenol with acetic acid. *J. Catal.* **226**, 308–320 (2004).
38. G. Kresse, J. Furthmüller, Efficient iterative schemes for ab initio total-energy calculations using a plane-wave basis set. *Phys. Rev. B Condens. Matter Mater. Phys.* **54**, 11169–11186 (1996).
39. P. E. Blöchl, Projector augmented-wave method. *Phys. Rev. B Condens. Matter Mater. Phys.* **50**, 17953–17979 (1994).
40. G. Kresse, D. Joubert, From ultrasoft pseudopotentials to the projector augmented-wave method. *Phys. Rev. B* **59**, 1758–1775 (1999).
41. S. Grimme, J. Antony, S. Ehrlich, H. Krieg, A consistent and accurate *ab initio* parametrization of density functional dispersion correction (DFT-D) for the 94 elements H-Pu. *J. Chem. Phys.* **132**, 154104 (2010).
42. S. Grimme, S. Ehrlich, L. Goerigk, Effect of the damping function in dispersion corrected density functional theory. *J. Comput. Chem.* **32**, 1456–1465 (2011).
43. G. Henkelman, B. P. Uberuaga, H. Jónsson, A climbing image nudged elastic band method for finding saddle points and minimum energy paths. *J. Chem. Phys.* **113**, 9901–9904 (2000).
44. A. Ghorbanpour, J. D. Rimer, L. C. Grabow, Periodic, vdW-corrected density functional theory investigation of the effect of Al siting in H-ZSM-5 on chemisorption properties and site-specific acidity. *Catal. Commun.* **52**, 98–102 (2014).
45. H. van Koningsveld, High-temperature (350 K) orthorhombic framework structure of zeolite H-Zsm-5. *Acta Crystallogr. B* **46**, 731–735 (1990).
46. L. García, G. Giannetto, M. R. Goldwasser, M. Guisnet, P. Magnoux, Phenol alkylation with methanol: Effect of sodium content and ammonia selective poisoning of an HY zeolite. *Catal. Lett.* **37**, 121–123 (1996).
47. J. A. Martens, M. Wydoodt, P. Espeel, P. A. Jacobs, Acid-catalyzed ketonization of mixtures of low carbon number carboxylic-acids on zeolite H-T. *Stud. Surf. Sci. Catal.* **78**, 527–534 (1993).

Acknowledgments

Funding: Flow reactions were supported by the U.S. Department of Energy (DOE) under grant DE-EE0006287 of the Bioenergy Technologies Office CHASE (Carbon, Hydrogen, and Separations Efficiencies) program. Catalyst characterization and theoretical calculations were supported by the DOE Experimental Program to Stimulate Competitive Research (grant DESC0004600). The calculations were performed at the Extreme Science and Engineering Discovery Environment and the OU Supercomputing Center for Education and Research at the University of Oklahoma. **Author contributions:** A.G. and S.C. designed the experiments. A.G. conducted all of the experiments. B.W. conducted all theoretical simulations. All authors contributed to the interpretation of the data and writing of the manuscript. **Competing interests:** The authors declare that they have no competing interests. **Data and materials availability:** All data needed to evaluate the conclusions in the paper are present in the paper and/or the Supplementary Materials. Additional data related to this paper may be requested from the authors.

Submitted 12 May 2016
Accepted 16 August 2016
Published 16 September 2016
10.1126/sciadv.1601072

Citation: A. Gumidyala, B. Wang, S. Crossley, Direct carbon-carbon coupling of furanics with acetic acid over Brønsted zeolites. *Sci. Adv.* **2**, e1601072 (2016).